 doi:10.20944/preprints201812.0210.v1

Common Connectivity Phenotypes in Rapid Eye Movement Sleep Behavior Disorder and Parkinson's Disease: The Search for an Intermediate Phenotype

Craig A. Moodie[1], Kelvin O. Lim[2,3], Bryon A. Mueller[3], Laura S. Hemmy[3], Michael J. Howell[4], Paul J. Tuite[4]

1 Department of Psychology, Stanford University

2 Department of Neuroscience, University of Minnesota Medical School

3 Department of Psychiatry, University of Minnesota Medical School

4 Department of Neurology, University of Minnesota Medical School

Corresponding Author: Paul J Tuite, 516 Delaware Street S.E. Minneapolis, MN 55455, tuite002@umn.edu

Number of words for Abstract: 200

Number of words for Article Body: 3755

Number of Figures: 8

Number of Tables: 0

Supplemental Information: 0

 doi:10.20944/preprints201812.0210.v1

Abstract

Rapid eye movement sleep behavior disorder (RBD) is often prodromal to Parkinson's disease (PD). Thus there should be detectable in vivo functional signatures shared between RBD and PD that aid in disease classification. To assess common in-vivo phenotypes, resting state data was collected on a 3T clinical MRI platform and a novel functional connectivity magnetic resonance imaging (fcMRI) approach, which combined independent component analysis (ICA) and graph theory, was used to evaluate deficits in interconnectivity among 15 PD, 14 RBD and 13 control participants. Whole brain and network-level analyses revealed the largest deficits in network connectivity in PD compared with controls, with less severe differences between RBD and controls. Importantly, the network-level analysis demonstrated decreased network interconnectivity, with the greatest aberrant networks in PD, and a subset in RBD. Additionally, a disease classification algorithm predicted PD cases by being trained on RBD cases with 0.87 sensitivity and 0.68 specificity. The functional alterations in cortical networks in RBD extended beyond the brainstem. These findings demonstrate progressive reductions in connectivity between brain networks, with less severe deficits in RBD than PD. Moreover, RBD phenotypes can be used to predict PD status in a cross-sectional sample, which suggests RBD is an intermediate phenotype.

Word Count: 200

Keywords:

Parkinson's, RBD, Connectivity, Phenotype, Classification, Network

 doi:10.20944/preprints201812.0210.v1

Introduction

Parkinson's disease (PD) is a neurodegenerative disorder characterized by progressive deposition of abnormal alpha-synuclein aggregates (i.e., synucleinopathy) that affects 1% of the population over the age of 60 years (Samii, Nutt, & Ransom, 2004). Several lines of evidence suggest that PD initially affects structures that relate to non-motor features such as the olfactory bulb: hyposmia, enteric plexus: constipation, and pons: rapid eye movement behavior disorder (RBD). Subsequently, the substantia nigra is affected which leads to the classic motor features, followed by cortical pathology resulting in cognitive decline (Borek, Amick, & Friedman, 2006; Braak, Ghebremedhin, Rub, Bratzke, & Del Tredici, 2004; Luk et al., 2013). RBD, a disorder of dream enactment, is often the heralding clinical feature of PD. Under non-pathological conditions, REM sleep is characterized by active mentation combined with skeletal muscle paralysis. In RBD, REM atonia is lost and patients will act out their dreams, often violently with thrashing, punching, and kicking. Previous studies have demonstrated that approximately 50% of individuals with RBD convert to PD or another synucleinopathy within a decade of diagnosis (Iranzo, Santamaria, & Tolosa, 2009; Postuma, Aarsland, et al., 2012; Schenck, Boeve, & Mahowald, 2013). Further, RBD combined with other non-motor features, such as anosmia and/or constipation, increase the risk of early conversion (Bezard & Fernagut, 2014).

Structural magnetic resonance techniques such as diffusion tensor imaging (DTI) have identified abnormalities in PD (Cho et al., 2010; Vaillancourt et al., 2009) as well as in RBD (Hanyu et al., 2012; Unger et al., 2010). While, resting state

 doi:10.20944/preprints201812.0210.v1

functional MRI has also demonstrated functional connectivity abnormalities in PD, for instance in the default mode network (van Eimeren, Monchi, Ballanger, & Strafella, 2009), fcMRI techniques are just now being applied to RBD (Ellmore et al., 2013) and have not been applied to comparisons of the two disorders. Dopamine-dependent differences in functional connectivity between the basal ganglia and cortex have also been found in PD (Williams et al., 2002; Yu, Liu, Wang, Chen, & Liu, 2013), and similar differences have also been reported for associations between several other brain regions, particularly cortical regions related to motor functioning (Sharman et al., 2012; Wu et al., 2011). It has been shown that these imaging phenotypes can predate the onset of impairments such as recognition memory deficits and, hence, imaging methods are being developed for in vivo classification of PD (Ibarretxe-bilbao et al., 2011; Long et al., 2012; Morales et al., 2012; Prodoehl et al., 2013).

As RBD is a prodromal syndrome of PD, we sought to evaluate alterations in connectivity among participants with RBD compared to PD as well as controls. Additionally, we sought to utilize ICA and graph theory as the means of capturing the functional networks and assessing their interconnectivity. ICA has been utilized as a powerful data-driven tool for deriving intrinsic connectivity networks (ICNs) from functional data, and graph theory has recently been used to describe the complex interactions between brain regions (Smith, 2012). Hence, the combination of these methodologies allows for the examination of the morphology and connectivity of the ICNs underlying the common phenotypes in PD and RBD, and could help establish RBD as an intermediate phenotype of PD. Finally, we were

 doi:10.20944/preprints201812.0210.v1

interested in whether the connectivity profile present in RBD could be used as an in vivo clinical classifier of disease state, as this provides a potential means for developing a tool for the early identification of PD in pre-motor or presymptomatic individuals.

 doi:10.20944/preprints201812.0210.v1

Materials and Methods

Participants

Fifteen individuals with PD, 14 individuals with idiopathic RBD and 13 controls (16 females, 26 males, mean age 60.0 ± 11.5) were included in this analysis from a larger sample recruited for a ^{123}I-Ioflupane (DaTSCAN) study to evaluate individuals with PD and those at risk for developing PD. The Institutional Review Board of the University of Minnesota approved all protocols and all participants gave informed consent before participating in the study. All participant information was de-identified at the beginning of the study and all participants were pre-screened using exclusionary criteria for both PD and idiopathic RBD.

All participants were initially assessed using the Unified PD Rating Scale (UPDRS)-based criteria (Poewe, Rascol, Sampaio, Stebbins, & Goetz, 2003). In addition, the enrolled PD patients all met the research diagnostic criteria established by the Queen Square Brain Bank (Brooks, 2012; Massano & Bhatia, 2012). All PD patients were medicated at the time of the study and did not have notable sleep disturbances. All RBD patients were diagnosed with a clinical history of dream enactment along with an in laboratory polysomnogram confirming REM sleep without atonia (AASM, 2001). RBD patients were excluded if the onset of dream enactment coincided with use of serotonergic antidepressant medication. Additionally, participants were excluded if they presented with a clinically significant acute or unstable physical or psychological disease on screening or in their history. In addition, exposure to investigational or radiological drugs within the 4 weeks prior to the scan was included as another exclusionary criteria. Control

Preprints (www.preprints.org) | NOT PEER-REVIEWED | Posted: 18 December 2018 doi:10.20944/preprints201812.0210.v1

subjects who were enrolled did not have a first degree relative with PD and were without a significant central nervous system neurological condition.

MR Acquisition and Imaging Parameters

A resting-state functional scan, a field map and high resolution T1 weighted anatomical images were acquired on a 3T Siemens TIM Trio MRI scanner using the system standard 12-channel receive-only head coil. For the resting state BOLD fMRI acquisition (EPI; TR=2000ms, TE=30ms, voxel size=3.4x3.4x4mm, matrix size=64x64, 34 AC-PC aligned single oblique axial slices with interleaved slice acquisition, 260 volumes, 9 min) the participants were instructed to close their eyes, remain awake, and not think about anything in particular. A field map acquisition (TR=300ms, TE=1.94/4.40ms, voxel and orientation matching fMRI scan, 1 min) was acquired just after the resting state scan. A structural T1-weighted image (MPRAGE, TR=2530ms, TE=3.65ms, TI=1100ms, flip angle=7 degrees, voxel size=1x1x1mm, 11 min) was collected and used for the anatomical registration of the functional scans.

Image Data Preprocessing

All data were preprocessed and analyzed with the FMRIB FSL 4.1.9 software (http://www.fmrib.ox.ac.uk/fsl). Preprocessing included the exclusion of the first 3 volumes to allow for magnetization stabilization, motion correction with the MCFLIRT linear registration algorithm (Jenkinson, Bannister, Brady, & Smith, 2002), B0 unwarping, interleaved slice-timing correction, brain extraction using the BET algorithm, spatial smoothing with a 5-mm full-width half-maximum Gaussian

 doi:10.20944/preprints201812.0210.v1

kernel, and high-pass temporal filtering. The images were registered to high-resolution T1 anatomical images and the MNI 2mm brain image using FLIRT.

FMRI Image Data Analysis

Intrinsic Connectivity Network (ICN) Generation

Data-driven ICA components were derived from the EPI functional scans using the FSL's temporal concatenation independent component analysis (TICA) software in the MELODIC ICA toolkit (Beckmann & Smith, 2004). This probabilistic TICA algorithm was used to generate global spatial maps and timeseries from the full matrix of voxel signals from scans from all participants. The MELODIC algorithm was constrained to thirty (30) components, which allowed for the standardization of the total number of components generated at the group and participant levels. The resulting components were subjected to a permutation procedure, which diminished any initial random value and participant-order effects (Wisner, Atluri, Lim, & MacDonald III, 2013).

The global ICA-derived components were then visually inspected and components that did not include neuronal signal, such as components with voxels outside the brain in the ventricles, were removed (Beckmann, 2012). The remaining components were identified as ICNs and were included in subsequent analyses. These global ICNs were then used as templates for back-transformation of individual-level spatial maps and timeseries with FSL's dual spatio-temporal regression software.

Signal Entropy, Connectivity Strength and Diversity

Preprints (www.preprints.org) | NOT PEER-REVIEWED | Posted: 18 December 2018 doi:10.20944/preprints201812.0210.v1

The individual-level, back-transformed ICN timeseries were used as the basis of the analysis of ICN time course entropy as well as all subsequent analyses. Univariate entropy here is defined as the Shannon entropy (Shannon, 1948) and is measured for each signal, i.e. within each ICN and then averaged across ICNs and participants within each group. For the bivariate metrics, the mean score for the i^{th} column of the connectivity matrix represents how well each node (ICN) is connected to all other nodes in the graph and, hence, the strength of the graph in this analysis is defined as the average strength across all ICNs. Similarly, the variance of the i^{th} column of the connectivity matrix represents the variability in the strength of connectivity for each ICN and, hence, the diversity is the average variability within group (Lynall et al., 2010).

Interconnectivity Analyses

To examine how well each individual network is connected with all other networks, we computed an *individual-level cross-correlation*. The individual-level ICN timeseries underwent an exhaustive cross-correlation procedure in which each ICN was correlated with every other ICN in order to produce correlation matrices. The cross-correlation scores were averaged across all participants per ICN within each group, and a statistical threshold based on the z-transformed overall ICN correlation values and sample size was used to determine which of the ICNs exhibited significant interconnectivity.

To determine mean interconnectivity differences across groups, ICN timeseries were concatenated across participants within each group in order to generate a group vector. In this *group-level cross-correlation* metric, these

 doi:10.20944/preprints201812.0210.v1

concatenated timeseries vectors were then all correlated within groups, and these scores were contrasted using a t-test. All group comparisons were done using a one-tailed alpha ($p < 0.05$), which was then corrected for the comparison of the three groups using a Bonferroni correction that yielded an adjusted "multivariate significance" alpha ($p < 0.017$).

Random Forests Prediction of Disease State

A random forest machine learning algorithm was employed to determine the accuracy of classification of group status between control, RBD and PD and, hence, disease severity. The forests were populated by decision trees which were trained to distinguish persons with RBD from controls using their scores for connectivity strength and diversity. This forest was then used to predict PD status based on the classes from the training data. Hence, the algorithm returned vectors of assignments for both the PD and control connectivity profiles, in which control was "0" and PD was "1". After group status was predicted using the classification algorithm, the two vectors of predicted and real scores were correlated. In addition, sensitivity and specificity were calculated using the following formulas:

$$\text{Sensitivity} = \text{true positives} / \text{true positives} + \text{false negatives}$$

$$\text{Specificity} = \text{true positives} / \text{true positives} + \text{false positives}$$

In order to provide an unbiased classification, the matrix of scores for controls was split into two test and train subgroups for the purposes of training and testing the classification algorithm. However, since the control subgroups were

 doi:10.20944/preprints201812.0210.v1

smaller than the training (RBD) and testing (PD), these subgroups were intermixed with another group of age matched controls, on which data had also been collected at the University of Minnesota. Hence, there were 10 subjects in the control training group, 14 subjects in the RBD training group, 10 subjects in the control testing group and 15 subjects in the PD testing group. There were no significant differences between the separate groups of controls in either demographics or connectivity scores.

3D Brain Figure Generation

All brain images were generated using Mango (the Multi-image Analysis GUI) viewer from the Research Imaging Institute of University of Texas Health Science Center (http://ric.uthscsa.edu/mango/index.html). All ICN overlays from the global ICA output were rendered on a 3D surface built off the MNI 152 T1 1-mm brain template. This 3D rendering was then made translucent to reveal the subsurface structures contained in each ICN. This was particularly important for sub-cortical structures such as the basal ganglia network or subgenual OFC & ACC network.

 doi:10.20944/preprints201812.0210.v1

Results

The UPDRS scores for the three groups were as follows: PD = 24.20 ± 9.24, RBD = 8.53 ± 5.82, control = 2.92 ± 2.53. The multi-group ICA, which was performed with data from all three groups, produced 22 common non-artifactual ICNs (Fig. 1). Of these 22 ICNs, 7 contained areas related to motor functioning, including the midbrain, cerebellum, primary motor cortex (M1) and corresponding somatosensory areas, pre-motor and supplementary regions, as well as the posterior parietal cortex. After all global maps were generated, these networks were also back-transformed into individual-level space in order to capture possible disease-relevant variance, which would be reflected as patient and control group differences.

In the univariate whole brain analysis, no significant differences were found in the entropy of the ICN timeseries when comparing the control and PD groups ($t = 1.09$, $df = 25.78$, $p = 0.14$, $d = 0.41$), the control and RBD groups ($t = 0.45$, $df = 15.59$, $p = 0.67$, $d = 0.17$), or RBD and PD groups ($t = 0.94$, $df = 16.65$, $p = 0.18$, $d = 0.36$) (Fig. 2). In the bivariate analyses, a significant difference was observed in connectivity strength between the control and PD groups ($t = 3.23$, $df = 22.73$, $p = 0.002$, $d = 1.24$), the difference between the control and RBD groups ($t = 2.05$, $df = 21.059$, $p = 0.027$, $d = 0.80$) was near significance after Bonferroni correction, and a weaker trend level difference was observed between the RBD and PD groups ($t = 1.57$, $df = 26.88$, $p = 0.06$, $d = 0.58$) (Fig. 3). For the diversity of connectivity, a significant difference was again found between the control and PD group ($t = 3.42$, $df = 25.49$, $p = 0.001$, $d = 1.29$). However, the comparisons of the control and RBD

Preprints (www.preprints.org) | NOT PEER-REVIEWED | Posted: 18 December 2018 doi:10.20944/preprints201812.0210.v1

groups (t = 1.91, df = 23.73, p = 0.03, d = 0.74) and the RBD and PD groups (t = 1.77, df = 26.77, p = 0.04, d = 0.65) were only at trend level after Bonferroni correction (Fig. 4).

Given that previous relationships have been established between signal entropy and the strength and diversity of connectivity (Bassett, Nelson, Mueller, Camchong, & Lim, 2012), these relationships were assessed and it was observed that there were indeed group differences in the scores for the Pearson correlation between strength and entropy (Fig. 5) and the Pearson correlation between diversity and entropy (Fig. 6). Significant group differences were observed for group comparisons between controls and PD (t = 3.03, df = 25.2, p = 0.003), controls and RBD (t = 2.33, df = 20.5, p = 0.015), but not PD vs RBD (t = 0.12, df = 24.37, p = 0.45) for the correlation between strength and entropy within group. For the t-tests of the scores from the Pearson's correlation of diversity and entropy per group, the comparison of the scores for the control and PD groups (t = 3.1, df = 23.28, p = 0.002) showed a significant group difference, but the scores of the control and RBD groups (t = 1.65, df = 18.55, p = 0.06) were not significantly different, neither were those for PD vs RBD groups (t = 0.73, df = 24.44, p-value = 0.24).

For the individual-level ICN cross-correlation, in the control group, 17 ICNs passed the threshold. For RBD, 14 ICNs passed threshold and were a subset of the 17 ICNs found in the controls. Similarly, for the PD group, only 10 ICNs passed threshold, which were again a subset of the 14 found in RBD group, and the larger set in controls (Figure 7).

 doi:10.20944/preprints201812.0210.v1

For the group-level cross-correlation, the t-test of interconnectivity scores showed that the control group had higher mean interconnectivity scores than both the PD group ($t = 4.16$, $df = 390.87$, $p = 0.00002$) and RBD group ($t = 2.00$, $df = 489.98$, $p = 0.023$), but the comparison of the control and RBD groups only had marginal multivariate significance ($p < .017$). In addition, it was observed that the RBD group had a higher group-level cross-correlation score when compared to the PD group ($t = 2.80$, $df = 547.09$, $p = 0.003$), even after Bonferroni correction.

The random forest classifier that was trained on a subgroup of controls versus RBD patients was tested on how well it could distinguish a separate group of controls from PD patients. It returned a vector of group assignments for controls (0) versus persons with Parkinson's disease (Figure 1). It was found that there was a correlation of $r = 0.69$ between the predicted and real scores, and the Parkinson's classification algorithm had a sensitivity of 0.87 and a specificity of 0.68.

 doi:10.20944/preprints201812.0210.v1

Discussion

The combined ICA - graph theory analyses of the connectivity profiles of the PD, RBD and control groups is a novel analysis strategy that is unlike seed-based approaches or typical ICA or graph theory analyses, in that it combines the data-driven network depiction of ICA and the descriptive power of graph theory to examine both global and network-level phenomena. Using this methodology, several metrics showed that there were significant differences between the three groups. Moreover, all the metrics revealed connectivity phenotypes in which the RBD group was intermediate between the PD and control groups, with a nested decrease in network interconnectivity going from controls to RBD to PD being the most striking finding.

In the univariate analysis of network entropy, there were no significant differences between the groups. However, this is not inconsistent with our previous findings of no significant differences in entropy related to disease state between persons with schizophrenia and controls (Bassett, Nelson, Mueller, Camchong, & Lim, 2011). Bivariate connectivity strength was strongest for controls, and less so for both the RBD and PD groups. Interestingly, while there was a significant connectivity strength difference between the control and PD groups, the differences between the control and PD group as well as PD and RBD groups were not significant after multiple comparison correction. Of note, the RBD group strength was in between that of the control and PD groups, thus suggesting an intermediate phenotype. These findings are consistent with other investigations that have demonstrated numerous subclinical abnormalities in cognitive functioning in

 doi:10.20944/preprints201812.0210.v1

persons who have not yet manifested PD (Fantini, Postuma, Montplaisir, & Ferini-strambi, 2006; Postuma, Gagnon, & Montplaisir, 2012; Postuma, Aarsland, et al., 2012).

For the bivariate analysis of diversity of connectivity, it was again found that diversity was highest for controls and lower for persons with both RBD and PD. Again, there was a trend showing that RBD was intermediate between controls and PD, but although the differences between the control and RBD as well as RBD and PD groups showed a strong trend, this did not reach significance after multiple comparison correction. In our previous analysis of connectivity diversity between controls and persons with schizophrenia, it was found that the schizophrenia group had significantly higher diversity than controls (Bassett et al., 2011), which contrasts with our findings in PD. This suggests that the diversity of connectivity is sensitive to different types of disease-related aberrations and, in schizophrenia, neuronal disorganization results in cognitive and behavioral deficits, as well as aberrant sensory and limbic processing, which is also reflected in an increase in connectivity diversity. In the case of PD, it is known that synuclein pathology often extends throughout the brain, which is then reflected in a decrease in connectivity diversity. In addition, the decrease in diversity demonstrated in RBD cases as compared to controls is consistent with the progressive deposition of alpha-synuclein pathology in brainstem and cortical regions.

While there were no significant group differences for signal entropy, the correlations between connectivity strength and signal entropy showed significant differences when comparing the control group to both the PD and RBD groups.

 doi:10.20944/preprints201812.0210.v1

Similarly, there was a significant difference between the control and PD groups for the correlation of entropy and diversity and this inverse association was again strongest for controls and weakest for the PD cases. This means that higher connectivity strength and diversity leads to lower signal entropy in a non-pathological state and this relationship is diminished with increasing pathology. Based upon this trend and our other connectivity findings we would suggest that the lack of significant group differences in entropy is simply due to a lack of power.

In the interconnectivity analysis, it was observed that, of all the 22 functional networks, 17 ICNs exhibited significant interconnectivity in the control group. Of these 17 networks, a subset of 14 exhibited significant interconnectivity for the RBD group, and an even smaller subset of 10 for the PD group. Hence, there was a nested decrease in interconnectivity between the PD, RBD and control groups, respectively. This observation was corroborated by the analysis of the canonical ICN timeseries per group, in which it was found that the mean interconnectivity was highest for the control group, significantly lower for the RBD group and, significantly lower still for the PD group. This group nesting implies that there is a common set of ICNs that generally have high interregional connectivity in healthy controls, but that some of these ICNs have decreased connectivity when individuals present with RBD, and that these same ICNs have deficient interconnectivity in the case of PD, in combination with an additional set of ICNs. Hence, this suggests that there is a common network-level deficit in both RBD and PD cases, but that this deficit is more severe for PD.

 doi:10.20944/preprints201812.0210.v1

To test this assertion, a random forests classifier was trained on a sample of RBD cases and controls and tested on its ability to identify PD cases. The high level of sensitivity and specificity that was obtained by this machine learning algorithm supports our findings that there is a sub-clinical state that is detectable in RBD and that is also informative of PD. While the accuracy was not perfect, we believe that as more information is gained about the in vivo states of both PD and its pre-clinical syndromes such as RBD, we will have greater predictive power to use phenotypes from the pre-clinical states to predict the onset of PD. However, the ultimate test will be to predict disease onset in pre-clinical patients in a longitudinal design in order to see how well these in vivo phenotypes can inform early detection models.

In conclusion, these findings demonstrate that there is a nested decrease in interconnectivity across RBD and PD, with increasing network dysfunction evident in a more advanced disease state (Ibarretxe-bilbao et al., 2011). Furthermore, we used these fcMRI metrics to detect increasing dysfunction in brain networks, as we used machine learning of the RBD connectivity profile to classify the PD connectivity profile. This finding is supported by a study in which regional fluctuation and synchronization differences between PD and controls allowed for blind separation of the two groups with good accuracy, specificity and sensitivity (Long et al., 2012). Hence, the interconnectivity phenotypes can serve as a possible biophysiological marker of disease progression even prior to the onset of relevant clinical symptoms, which make these metrics potentially useful in clinical trials.

 doi:10.20944/preprints201812.0210.v1

Acknowledgements: Preliminary data from this project was presented at the International REM Sleep Behavior Disorder Study Group Meeting in Valencia, Spain (October 2013) and the Organization for Human Brain Mapping Annual Meeting in Hamburg, Germany (June 2014). Data collection for this study was supported by a grant from GE Healthcare, Inc., grant number 10-DAT-003. The authors are grateful to Christa Raszkowski for her assistance with the recruitment of participants for this study and for all participants who made this study possible.

Author Contributions:

Conceptualization, Paul Tuite, Laura Hemmy, Kelvin Lim and Michael Howell; Data curation, Laura Hemmy, Michael Howell and Bryon Mueller; Formal analysis, Craig Moodie, Laura Hemmy and Bryon Mueller; Funding acquisition, Paul Tuite; Investigation, Paul Tuite, Craig Moodie, Laura Hemmy, Kelvin Lim, Michael Howell and Bryon Mueller; Methodology, Paul Tuite, Laura Hemmy, Michael Howell and Bryon Mueller; Project administration, Paul Tuite, Laura Hemmy and Kelvin Lim; Resources, Laura Hemmy and Michael Howell; Software, Craig Moodie, Laura Hemmy, Kelvin Lim and Bryon Mueller; Supervision, Paul Tuite and Kelvin Lim; Validation, Laura Hemmy; Writing – original draft, Craig Moodie; Writing – review & editing, Paul Tuite, Craig Moodie, Laura Hemmy, Kelvin Lim, Michael Howell and Bryon Mueller.

 doi:10.20944/preprints201812.0210.v1

Financial Disclosures: Data collection for this study was supported by a grant from GE Healthcare, Inc., grant number 10-DAT-003. Paul Tuite, the senior author on this paper also received funding from the National Institutes of Health (NIH) and Northwestern University for evaluation of isradipine, NIH for being part of the Udall Parkinson Centers, Michael J. Fox foundation for the Biofind study and funding from Biogen and Bristol-Myers Squibb for evaluation of tau-directed monoclonal antibody BIIB092 for progressive supranuclear palsy. Dr. Tuite had been supported by a grant from the UK Parkinson's Organization to evaluate N-acetylcysteine in a clinical trial.. The other authors have no other conflicts of interest, financial or otherwise, to declare.

References

1. AASM. (2001). *THE INTERNATIONAL CLASSIFICATION OF SLEEP DISORDERS, REVISED: Diagnostic and Coding Manual*. Westchester, IL: American Academy of Sleep Medicine.
2. Bassett, D. S., Nelson, B. G., Mueller, B. A., Camchong, J., & Lim, K. O. (2011). Altered resting state complexity in schizophrenia. *Neuroimage*. Retrieved from http://www.hubmed.org/display.cgi?uids=22008374
3. Beckmann, C. F. (2012). Modelling with independent components. *NeuroImage*, *62*(2), 891–901. doi:10.1016/j.neuroimage.2012.02.020
4. Beckmann, C., & Smith, S. (2004). Probabilistic independent component analysis for functional magnetic resonance imaging. *Institute of Electrical and Electronics Engineers Transactions on Medical Imaging*, *23*(2), 137–52. Retrieved from http://ieeexplore.ieee.org/xpls/abs_all.jsp?arnumber=1263605
5. Bezard, E., & Fernagut, P.-O. (2014). Premotor parkinsonism models. *Parkinsonism & Related Disorders*, *20S1*, S17–S19. doi:10.1016/S1353-8020(13)70007-5
6. Borek, L., Amick, M., & Friedman, J. (2006). Non-motor aspects of Parkinson's disease. *CNS Spectrums*, *7*(July). Retrieved from http://mbldownloads.com/0706CNS_Borek_CME.pdf
7. Braak, H., Ghebremedhin, E., Rub, U., Bratzke, H., & Del Tredici, K. (2004). Stages in the development of Parkinson's disease-related pathology. *Cell Tissue Res*, *318*, 121–134.
8. Brooks, D. J. (2012). Parkinson's disease: Diagnosis. *Parkinsonism and Realted Disorders*, *18*, S31–S33. doi:10.1016/S1353-8020(11)70012-8
9. Cho, Z., Oh, S., Kim, J., Park, S.-Y., Kwon, D.-H., Jeong, H.-J., … Jeon, B. S. (2010). Direct Visualization of Parkinson ' s Disease by In Vivo Human Brain Imaging Using 7 . 0T Magnetic Resonance Imaging. *Movement Disorders*, *xx*(xxx), 1–6. doi:10.1002/23465
10. Ellmore, T. M., Castriotta, R. J., Hendley, K. L., Aalbers, B. M., Furr-stimming, E., Hood, A. J., … Schiess, M. C. (2013). Altered Nigrostriatal and Nigrocortical Functional Connectivity in Rapid Eye Movement Sleep Behavior Disorder. *Sleep*, *36*(12), 1885–1892.
11. Fantini, M. L., Postuma, R. B., Montplaisir, J., & Ferini-strambi, L. (2006). Olfactory deficit in idiopathic rapid eye movements sleep behavior disorder. *Brain Research Bulletin*, *70*, 386–390. doi:10.1016/j.brainresbull.2006.07.008
12. Hanyu, H., Inoue, Y., Sakurai, H., Kanetaka, H., Nakamura, M., Miyamoto, T., … Iwamoto, T. (2012). Parkinsonism and Related Disorders Voxel-based magnetic resonance imaging study of structural brain changes in patients with idiopathic REM sleep behavior disorder. *Parkinsonism and Related Disorders*, *18*(2), 136–139. doi:10.1016/j.parkreldis.2011.08.023
13. Ibarretxe-bilbao, N., Zarei, M., Junque, C., Jose, M., Segura, B., Vendrell, P., … Tolosa, E. (2011). NeuroImage Dysfunctions of cerebral networks precede recognition memory deficits in early Parkinson ' s disease. *NeuroImage*, *57*(2), 589–597. doi:10.1016/j.neuroimage.2011.04.049

14. Iranzo, A., Santamaria, J., & Tolosa, E. (2009). The clinical and pathophysiological relevance of REM sleep behavior disorder in neurodegenerative diseases. *Sleep Medicine Reviews*, *13*(6), 385–401. doi:10.1016/j.smrv.2008.11.003
15. Jenkinson, M., Bannister, P., Brady, M., & Smith, S. (2002). Improved Optimization for the Robust and Accurate Linear Registration and Motion Correction of Brain Images. *NeuroImage*, *17*, 825–841. doi:10.1006/nimg.2002.1132
16. Long, D., Wang, J., Xuan, M., Gu, Q., Xu, X., Kong, D., & Zhang, M. (2012). Automatic Classification of Early Parkinson's Disease with Multi-Modal MR Imaging. *PloS One*, *7*(11), 1–9. doi:10.1371/journal.pone.0047714
17. Luk, K. C., Kehm, V., Carroll, J., Zhang, B., Brien, P. O., Trojanowski, J. Q., & Lee, V. M.-Y. (2013). Pathological α-Synuclein Transmission Initiates Parkinson-like Neurodegeneration in Non-transgenic Mice. *Science*, *338*(6109), 949–953. doi:10.1126/science.1227157.Pathological
18. Lynall, M., Bassett, D. S., Kerwin, R., Mckenna, P. J., Kitzbichler, M., Muller, U., & Bullmore, E. (2010). Functional Connectivity and Brain Networks in Schizophrenia. *The Journal of Neuroscience*, *30*(28), 9477–9487. doi:10.1523/JNEUROSCI.0333-10.2010
19. Massano, J., & Bhatia, K. P. (2012). Clinical approach to Parkinson's disease: features, diagnosis, and principles of management. *Cold Spring Harbor Perspectives in Medicine*, *2*(6), 1–15. doi:10.1101/cshperspect.a008870
20. Morales, D. A., Vives-Gilabert, Y., Gomez-Ansond, B., Bengoetxea, E., Larranaga, P., Bielza, C., … Delfino, M. (2012). Predicting dementia development in Parkinson's disease using Bayesian network classifiers. *Psychiatry Research: Neuroimaging*, 1–7. doi:10.1016/j.pscychresns.2012.06.001
21. Poewe, W., Rascol, O., Sampaio, C., Stebbins, G. T., & Goetz, C. G. (2003). The Unified Parkinson's Disease Rating Scale (UPDRS): Status and Recommendations. *Movement Disorders*, *18*(7), 738–750. Retrieved from http://www.ncbi.nlm.nih.gov/books/NBK27754/
22. Postuma, R. B., Aarsland, D., Barone, P., Burn, D., Hawkes, C., Oertel, W., & Ziemssen, T. (2012). Identifying Prodromal Parkinson's Disease: Pre-Motor Disorders in Parkinson's Disease. *Movement Disorders*, *27*(5), 617–626. doi:10.1002/mds.24996
23. Postuma, R. B., Gagnon, J., & Montplaisir, J. Y. (2012). REM sleep behavior disorder: From dreams to neurodegeneration. *Neurobiology of Disease*, *46*(3), 553–558. doi:10.1016/j.nbd.2011.10.003
24. Prodoehl, J., Li, H., Planetta, P. J., Goetz, C. G., Shannon, K. M., Tangonan, R., … Vaillancourt, D. E. (2013). Diffusion Tensor Imaging of Parkinson's Disease, Atypical Parkinsonism, and Essential Tremor. *Movement Disorders*, *28*(13), 1816–1822. doi:10.1002/mds.25491
25. Samii, A., Nutt, J. G., & Ransom, B. R. (2004). Parkinson's disease. *The Lancet*, *363*, 1783–1793.
26. Schenck, C. H., Boeve, B. F., & Mahowald, M. W. (2013). Delayed emergence of a parkinsonian disorder or dementia in 81 % of older males initially diagnosed with idiopathic REM sleep behavior disorder (RBD): 16 year update on a

previously reported series. *SLEEP MEDICINE*, 1–5. doi:10.1016/j.sleep.2012.10.009

27. Shannon, C. E. (1948). A Mathematical Theory of Communication. *Bell System Technical Journal*, *27*(3), 379–423.
28. Sharman, M., Valabregue, R., Perlbarg, V., Marrakchi-Kacem, L., Vidailhet, M., Benali, H., … Lehericy, S. (2012). Parkinson's Disease Patients Show Reduced Cortical-Subcortical Sensorimotor Connectivity. *Movement Disorders*, *28*(4), 447–454. doi:10.1002/mds.25255
29. Smith, S. M. (2012). The future of FMRI connectivity. *NeuroImage*, *62*(2), 1257–66. doi:10.1016/j.neuroimage.2012.01.022
30. Unger, M. M., Belke, M., Menzler, K., Heverhagen, J. T., Keil, B., Stiasny-kolster, K., & Rosenow, F. (2010). Diffusion Tensor Imaging in Idiopathic REM Sleep Behavior Disorder Reveals Microstructural Changes in the Brainstem , Substantia Nigra , Olfactory Region , and Other Brain Regions. *Sleep*, *33*(6), 767–773.
31. Vaillancourt, D. E., Spraker, M. B., Prodoehl, J., Abraham, I., Corcos, D. M., Zhou, X. J., & Al., E. (2009). High-resolution diffusion tensor imaging in the substantia nigra of de novo Parkinson disease. *Neurology.*, *72*((16)), 1378–84.
32. Van Eimeren, T., Monchi, O., Ballanger, B., & Strafella, A. P. (2009). Dysfunction of the Default Mode Network in Parkinson Disease : *Archives of Neurology*, *66*(7), 877–883. doi:10.1001/archneurol.2009.97.Dysfunction
33. Williams, D., Tijssen, M., Bruggen, G. Van, Bosch, A., Insola, A., Lazzaro, V. Di, … Brown, P. (2002). Dopamine-dependent changes in the functional connectivity between basal ganglia and cerebral cortex in humans. *Brain*, *125*, 1558–1569. Retrieved from http://brain.oxfordjournals.org/content/125/7/1558.short
34. Wisner, K., Atluri, G., Lim, K., & MacDonald III, A. (2013). Neurometrics of intrinsic connectivity networks at rest using fMRI: Retest reliability and cross-validation using a meta-level method. *NeuroImage*, *76*, 236–51. Retrieved from http://www.sciencedirect.com/science/article/pii/S1053811913002218
35. Wu, T., Long, X., Wang, L., Hallett, M., Zang, Y., Li, K., & Chan, P. (2011). Functional Connectivity of Cortical Motor Areas in the Resting State in Parkinson's Disease. *Human Brain Mapping*, *32*, 1443–1457. doi:10.1002/hbm.21118
36. Yu, R., Liu, B., Wang, L., Chen, J., & Liu, X. (2013). Enhanced Functional Connectivity between Putamen and Supplementary Motor Area in Parkinson's Disease Patients. *PloS One*, *8*(3), e59717. doi:10.1371/journal.pone.0059717

 doi:10.20944/preprints201812.0210.v1

Figure Captions

Figure 1. 3D overlays of spatial maps from intrinsic connectivity networks (ICNs) generated from the independent component analysis of fMRI data from the Parkinson's disease (PD), rapid eye movement sleep behavior disorder (RBD) and control groups. Global spatial maps were derived and thresholded (z = 6) and rendered in either axial or coronal orientations.

Figure 2. Box plot showing group differences in the intrinsic connectivity networks' (ICN) timeseries entropy between the three groups. Entropy here is defined as the Shannon entropy (see methods).

Figure 3. Box plot showing group differences in connectivity strength between the three groups. Significance thresholds were established using one-tailed t-tests and corrected for multiple comparisons ($p < 0.017$).

Figure 4. Box plot showing group differences in connectivity diversity between the three groups. Significance thresholds were established using one-tailed t-tests and corrected for multiple comparisons ($p < 0.017$).

Figure 5. Box plot showing group differences in the Pearson correlations of connectivity strength and intrinsic connectivity network (ICN) timeseries entropy between the three groups. Significance thresholds were established using one-tailed t-tests and corrected for multiple comparisons ($p < 0.017$).

Preprints (www.preprints.org) | NOT PEER-REVIEWED | Posted: 18 December 2018 doi:10.20944/preprints201812.0210.v1

Figure 6. Box plot showing group differences in the Pearson correlations of connectivity diversity and intrinsic connectivity network (ICN) timeseries entropy between the three groups. Significance thresholds were established using one-tailed t-tests and corrected for multiple comparisons ($p < 0.017$).

Figure 7. 3D rendering of intrinsic connectivity networks (ICNs) exhibiting significant interconnectivity within the three groups. The set of 17 ICNs shown in the figure all showed significant interconnectivity in the control group, as depicted by the yellow bars. A subset, comprised of 14 of these ICNs, had significant interconnectivity in the RBD group and is labeled using the green bars. A smaller subset (10 ICNs) also exhibited significant interconnectivity in the PD group, as shown by the orange bars.

Figure 8. Bar graph depiction of the results from a random forests prediction of Parkinson's disease cases based on connectivity phenotypes from RBD. Decision trees were trained to identify RBD and control cases using their respective connectivity strength and diversity profiles and then tested for their ability to distinguish a separate set of controls from PD patients. The number of predicted cases is plotted on the y-axis and the groups (control = "0", PD = "1") are on the x-axis.

Preprints (www.preprints.org) | NOT PEER-REVIEWED | Posted: 18 December 2018 doi:10.20944/preprints201812.0210.v1

Figures

Figure 1. ICA-derived ICNs used in graph theory analyses

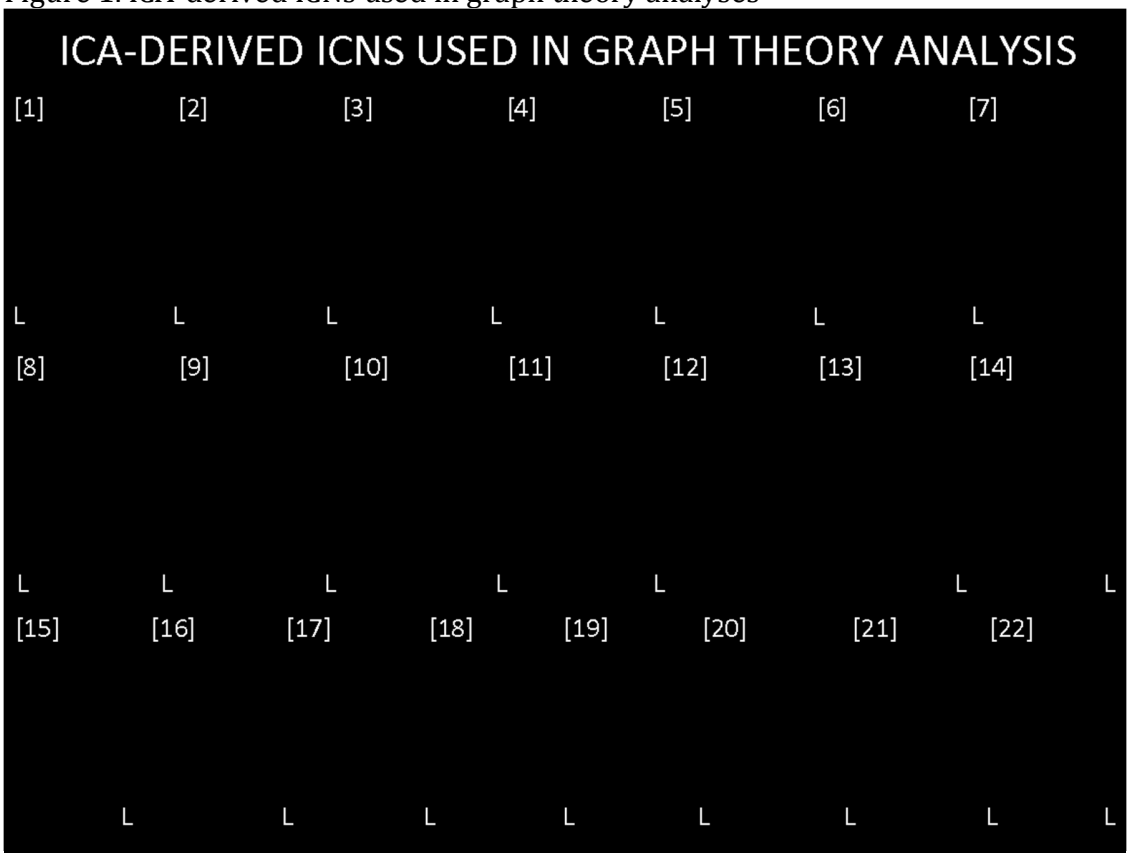

Figure 2. Univariate Entropy

Preprints (www.preprints.org) | NOT PEER-REVIEWED | Posted: 18 December 2018 doi:10.20944/preprints201812.0210.v1

Figure 3. Bivariate Strength

Figure 4. Bivariate Diversity

Preprints (www.preprints.org) | NOT PEER-REVIEWED | Posted: 18 December 2018 doi:10.20944/preprints201812.0210.v1

Figure 5. Pearson's Correlation between Strength and Entropy

Figure 6. Pearson's Correlation between Diversity and Entropy

Preprints (www.preprints.org) | NOT PEER-REVIEWED | Posted: 18 December 2018 doi:10.20944/preprints201812.0210.v1

Figure 7. ICNs exhibiting significant interconnectivity

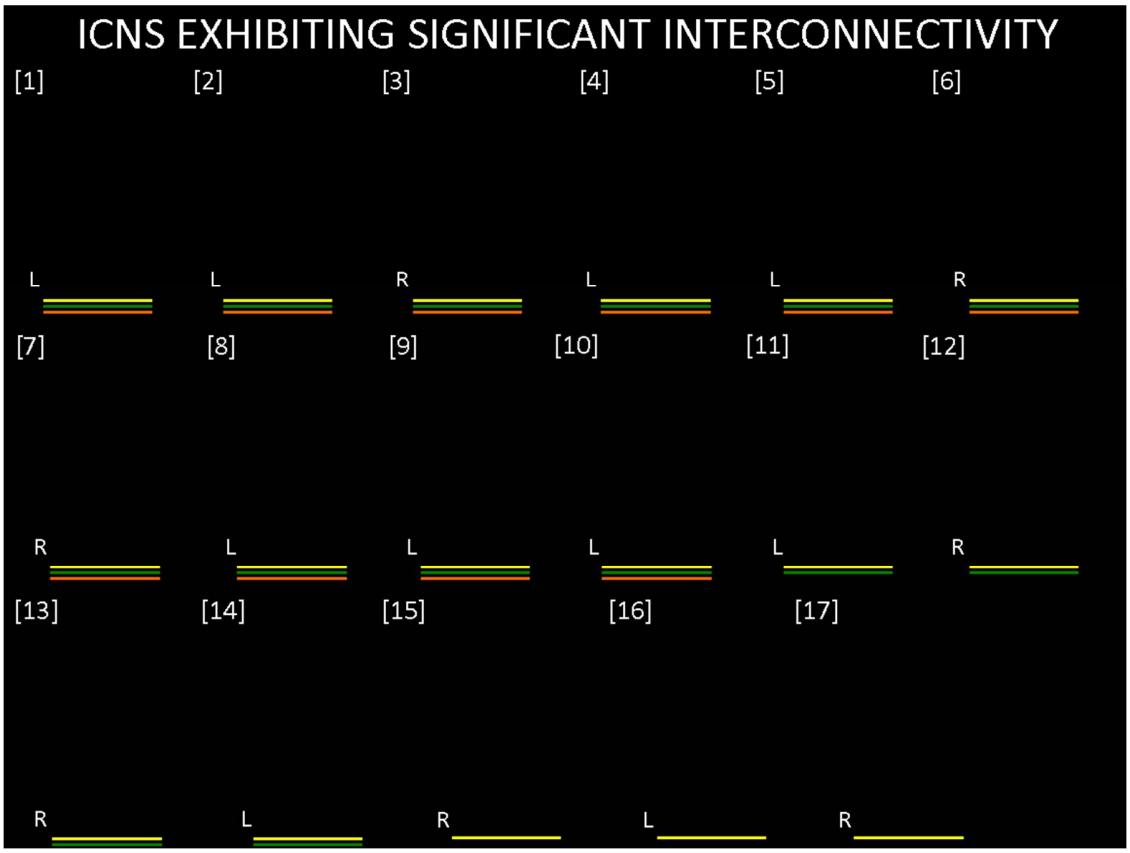

Preprints (www.preprints.org) | NOT PEER-REVIEWED | Posted: 18 December 2018 doi:10.20944/preprints201812.0210.v1

Figure 8. Classification of PD subjects using random forests trained on RBD cases